Technical Report
DL-TR-95-002

Spin-Resolved Electron Spectroscopy on the SRS

I W Kirkman E A Seddon and F M Quinn

August 1995

COUNCIL FOR THE CENTRAL LABORATORY OF THE RESEARCH COUNCILS

Enquiries about copyright, reproduction and requests for additional copies of this report should be addressed to:

The Central Laboratory for the Research Councils
Chadwick Library
Daresbury Laboratory
Daresbury
Warrington
Cheshire
WA4 4AD
Tel: 01925 603397 Fax: 01925 603195
E-mail library@dl.ac.uk

ISSN 1358-6254

SPIN-RESOLVED ELECTRON SPECTROSCOPY ON THE SRS

I.W. Kirkman, E.A. Seddon* and F.M. Quinn

Abstract

This document summarises some of the techniques used, and the equipment available, for spin-resolved electron spectroscopy at Daresbury Laboratory. An introduction to Mott scattering is first given, then the experimental arrangements and procedures adopted on both Station 1.2 and the 'Micro-Mott' facility are described. Details of the data processing and analysis are given, followed by some examples of experimental results. Emphasis is placed upon the methods adopted for removing instrumental effects, which are of particular significance for this field of study.

1 Introduction

As early as 1929 Sir Nevill Mott presented the arguments for the impossibility of separating free electrons of different spin by performing a Stern-Gerlach type experiment[1]. Fortunately, he went on to suggest[2] an alternative experimental technique, based on high energy scattering, that could be used - a suggestion that has prompted a great deal of experimental activity[3]. So-called Mott scattering was first successfully used to determine the polarisation of electron beams some 13 years later in 1942[4]. It has been in use ever since and is therefore a well tried and tested though not easy technique[5].

Mott scattering is sensitive to beam polarisations because spin-orbit coupling induces a spin dependence in the scattering potential and hence in the scattering cross section. Experimentally, the technique involves the bombardment of heavy nuclei targets with an energetic (100keV) electron beam and the detection of those electrons scattered through large angles by strategically placed detectors. An electron beam of polarisation P, when

* Author to whom any queries should be addressed.

back-scattered from a thin gold foil, will show a small left-right asymmetry, A, in the normalised scattered intensity.

A is defined as:

$$A = (L-R) / (L+R) \qquad [1]$$

where L and R are the left and right count rates respectively. P is related to A by the simple expression:

$$A = S_{eff} . P \qquad [2]$$

Where S_{eff}, the effective Sherman Function of the instrument, can be interpreted as a measure of the spin sensitivity of the polarimeter. The angular dependence of S_{eff}[6], shown in Fig. 1, leads directly to the optimum backward scattering detector placement angle of 120° (relative to the direction of the incoming beam).

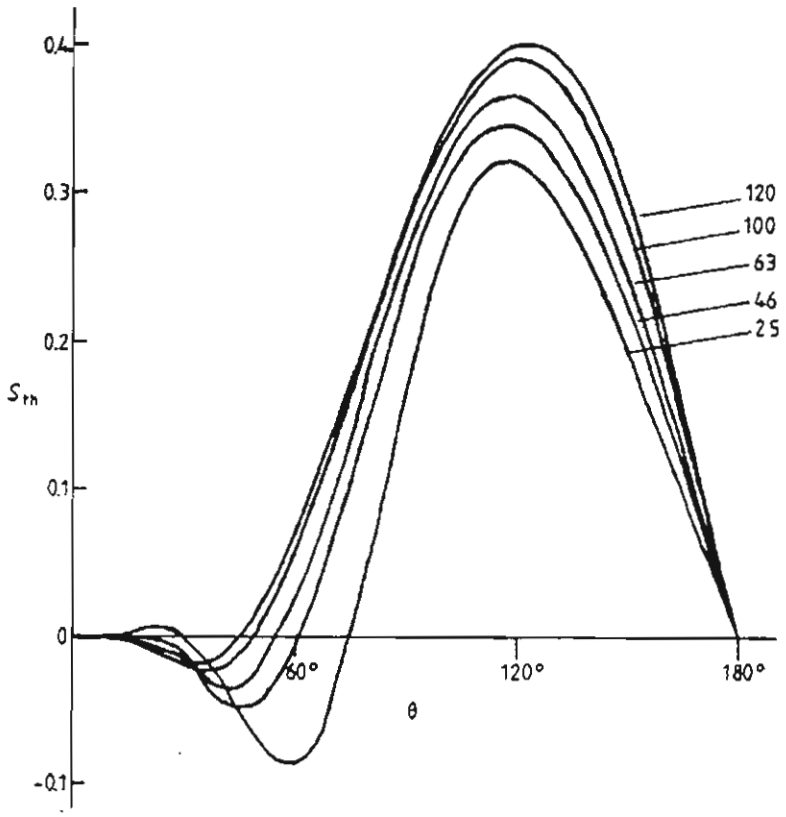

Figure 1 : The Angular Dependence of S_{eff}

High energy Mott scattering is, of course, not the only technique currently available for the determination of electron beam polarisations, and reviews by Unguris *et al.*[7] and Gay and Dunning[5] have helped to put the various techniques into context.

Two experimental facilities for use with polarised electrons have been developed for use on the SRS. The first is a dedicated beamline and station, Station 1.2, which incorporates a conventional high-energy Mott polarimeter for spin analysis of electrons photoemitted from surfaces under UHV conditions. The second is an energy and angle resolving instrument which incorporates a conical retarding potential Mott polarimeter (the "Micro-Mott" facility) for use in a variety of configurations on a number of beamlines. These facilities have been the subject of previous reports[8] [9] [10].

2 The Mott Polarimeter on Station 1.2

The high energy Mott polarimeter and its relation to the rest of Station 1.2 is shown schematically in Fig. 2. Essentially, the photoemitted electrons emergent at 45° to the incident photon beam are energy analysed in a hemispherical analyser, they then undergo acceleration (to 3keV) and focusing to a small spot at the entrance to the deflection magnet. After deflection the electrons are electrostatically accelerated to 100keV and focused to a spot approximately 1mm across on a gold scattering target within the polarimeter.

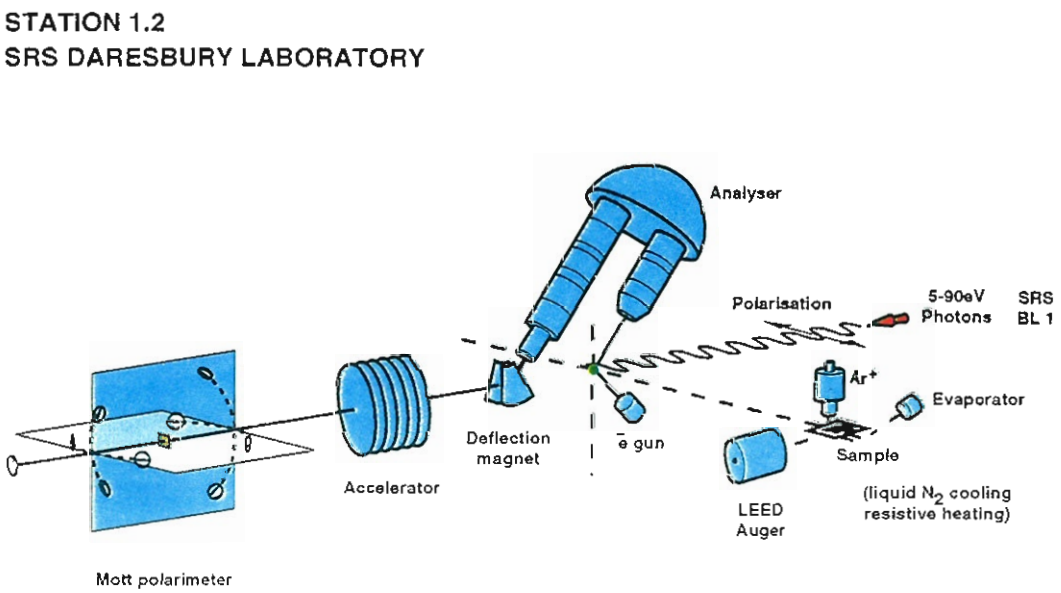

Figure 2 : Schematic Representation of Station 1.2 on the SRS

A photograph of the high energy Mott polarimeter is shown in Fig. 3. It consists of an array of nine surface barrier detectors - shown as discs in Fig. 2. The four backward detectors (also referred to as *polarisation* detectors) detect electrons scattered over an angular range of 110-130°, where - as clearly shown in Fig. 1 - the spin-dependent scattering asymmetry for 100keV electrons is calculated to be at its peak of around 35%. Four forward detectors (also referred to as *monitor* detectors) detect electrons over the range 10-14° where the spin dependent scattering asymmetry is calculated to be less than 1%. A further forward detector

is placed directly on the axis of the incident beam. The electrons are scattered from gold foils held in a motor driven foil holder that currently supports three thicknesses of foil (of 300, 600 and 1000Å), an uncoated Lexan™ backing film and a clear aperture. The whole assembly mounts on a ten inch flange which can be seen to the right of the ion pump port in the centre of the anti-corona housing of the Mott polarimeter depicted in Fig. 4. When operating, the chamber housing the polarimeter is at high voltage - routinely 100kV- it is therefore subject to stringent safety precautions.

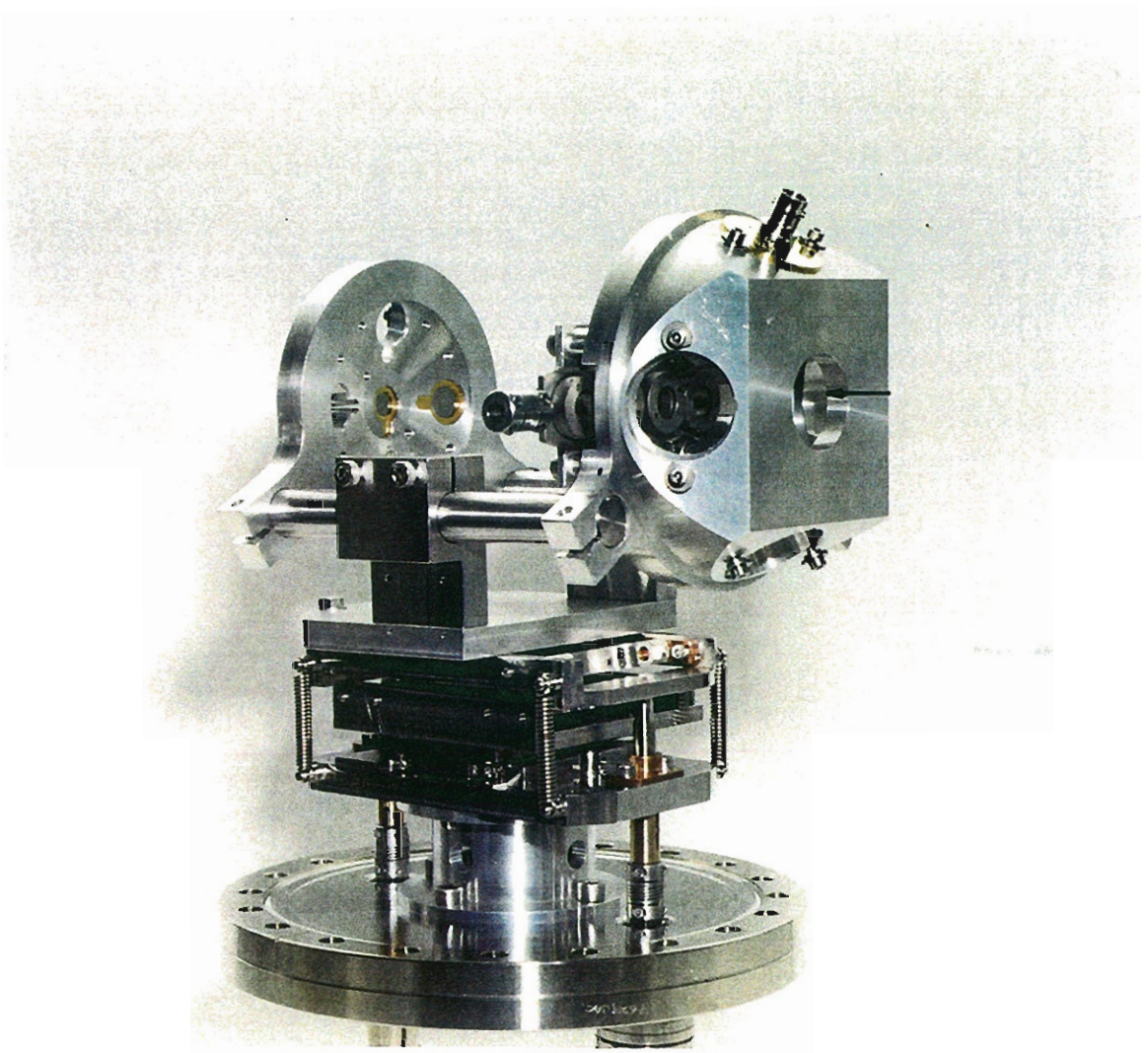

Figure 3 : Internal Arrangement of the Array of 9 Silicon Surface Barrier Detectors within the High-Energy Mott Polarimeter

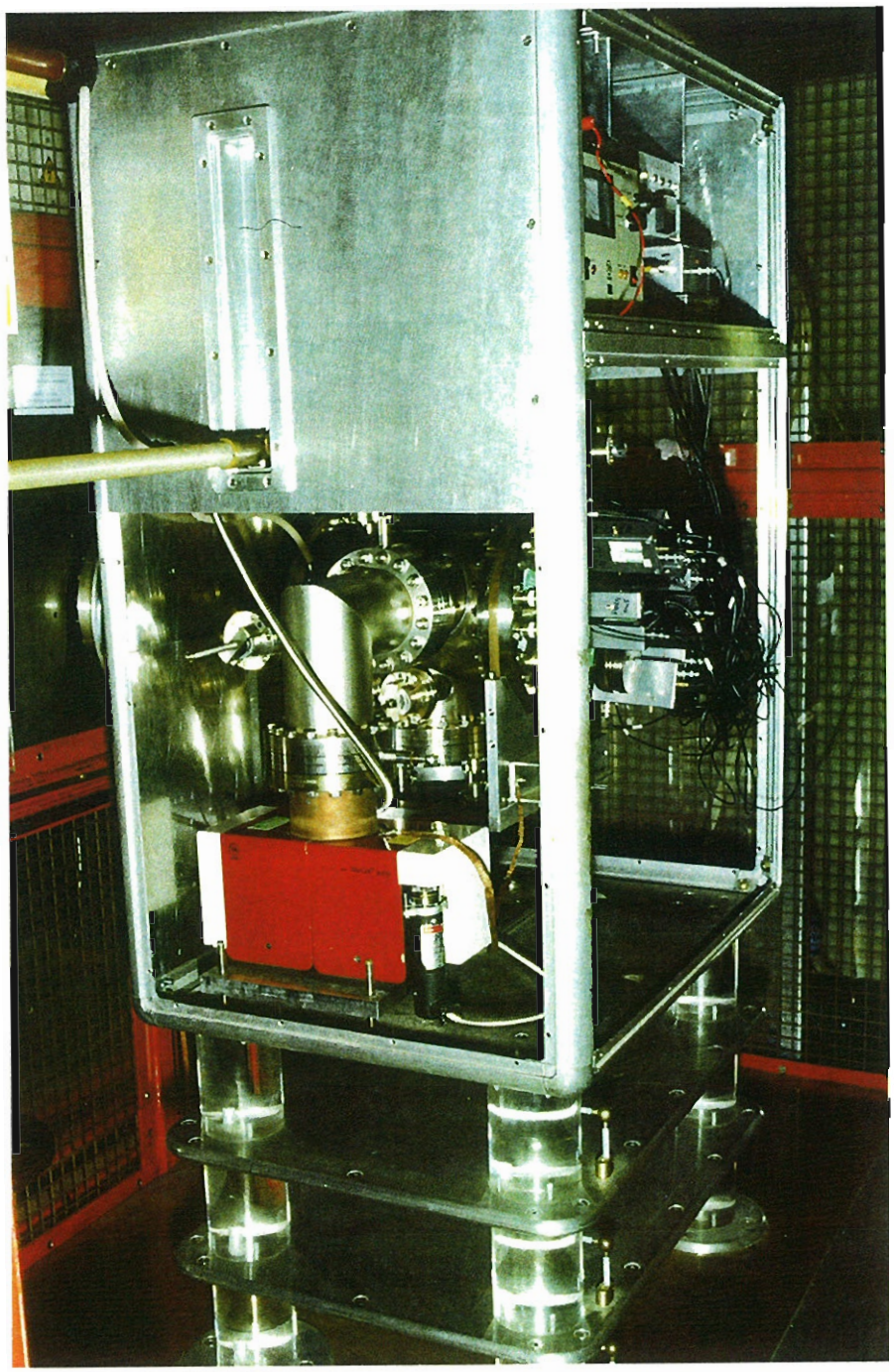

Figure 4 :The External View of the High-Energy Mott Polarimeter

The data acquisition chain is shown schematically in Fig. 5. The charge pulses generated in the barrier detectors are fed into charge sensitive amplifiers (Amptek, A225), each arranged to have a gain of 10. The signal pulses then pass into two stage amplifier/discriminator chips (Amptek, A206) which provide a further gain of 10. Both chips are housed in small units which are mounted directly onto feedthroughs on the end flange of the Mott polarimeter (see Fig. 4) and are therefore also at a potential of 100kV when the polarimeter is in operation. The signals from these are coupled to equipment at ground potential using fibre optic cables. The TTL signal pulses are passed to the counter/timers (Microlink EC8 units), and data

collection and processing takes place on an IBM compatible computer (Viglen 386). Further technical details of the data acquisition and control system are to be reported elsewhere[11] [12].

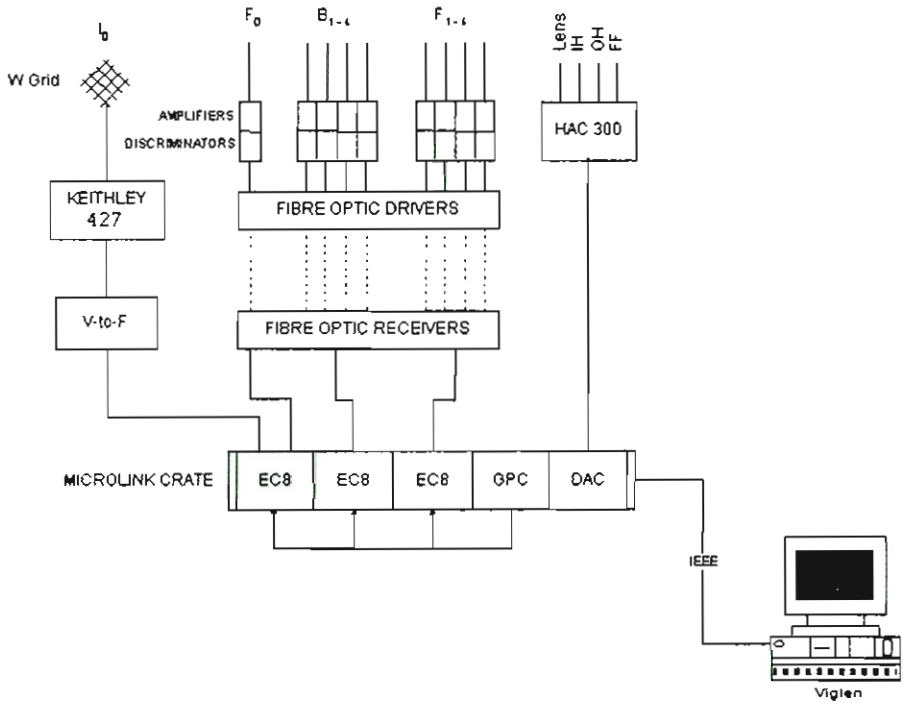

Figure 5 : Schematic Representation of the Data Acquisition Chain for Station 1.2

3 The 'Micro-Mott' Facility

The concept of a retarding potential Mott polarimeter was suggested by Farago and first realised by Dunning and co-workers[13] in 1979. The device works on the same principle of spin-orbit induced asymmetric scattering that is the physical basis of high energy Mott polarimeters, but the electron beam is only accelerated to around 20keV before scattering from a thick heavy element target and the scattered electrons are decelerated to close to ground potential before they are detected using channeltrons or channel plates. The latest generation of this type of polarimeter have conical geometry and are known as Micro-Mott polarimeters owing to their relatively small size.

Two priority applications were identified for the facility, those of spin- and angle-resolved photoemission; a) from atomic and molecular species under high vacuum conditions, and b) from condensed matter under UHV conditions. Both of these applications require energy analysis of the photoelectrons. A four detector polarimeter, depicted in Fig. 6, was therefore mounted on a small (50mm radius) hemispherical analyser (shown schematically in Fig. 7) and the whole assembly was mounted either on a special bracket for gas phase work or a two circle goniometer for condensed matter work. This latter option is illustrated in Fig. 8. The polarimeter/analyser assembly and associated wiring *etc.* was constructed from UHV compatible materials so that there would be minimal interconversion downtime between the two types of application.

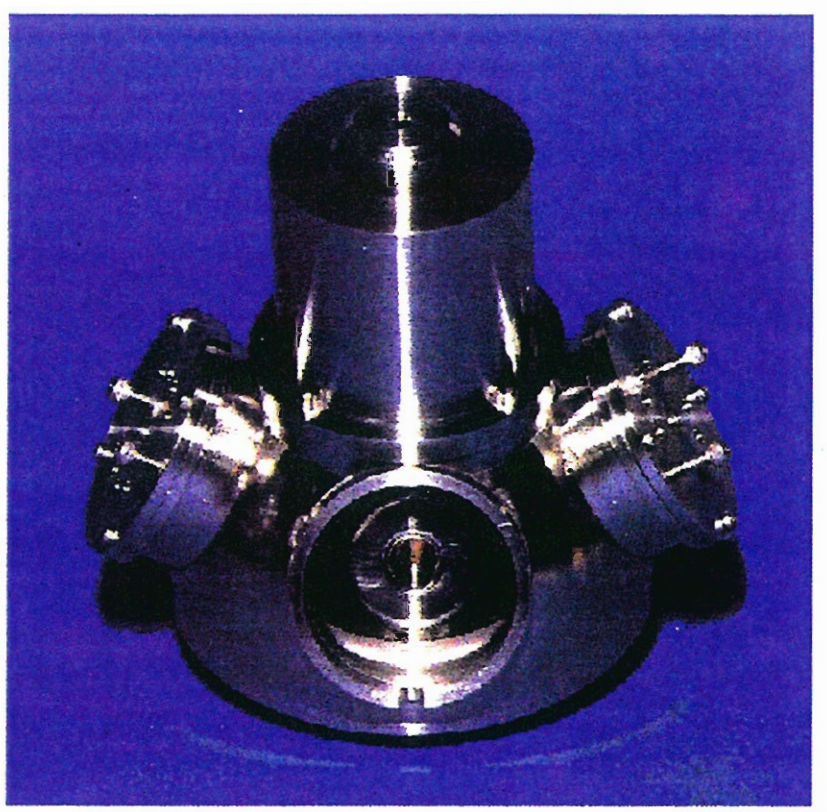

Figure 6 : Photograph of the Micro-Mott Polarimeter

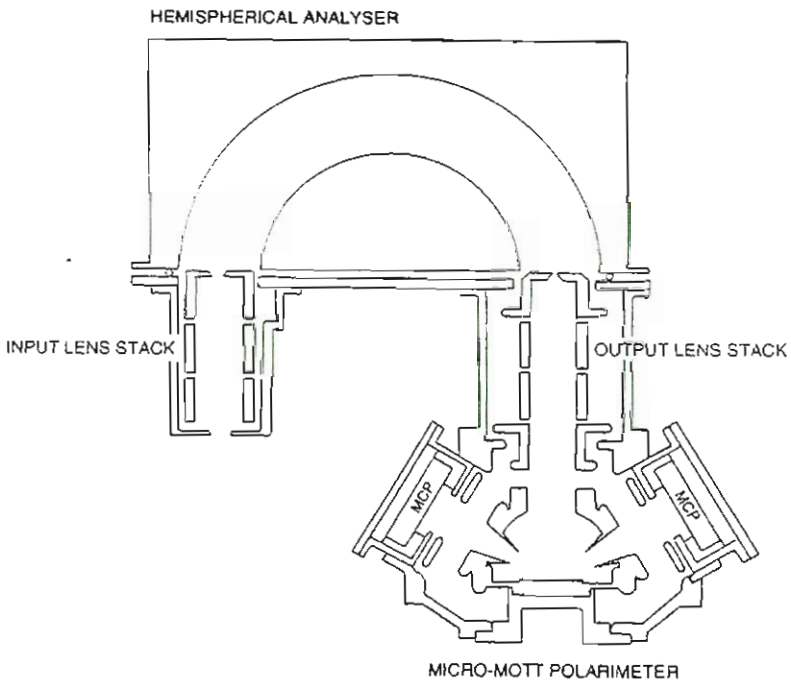

Figure 7 : Schematic Diagram of the Micro-Mott Polarimeter/Electron Energy Analyser Assembly

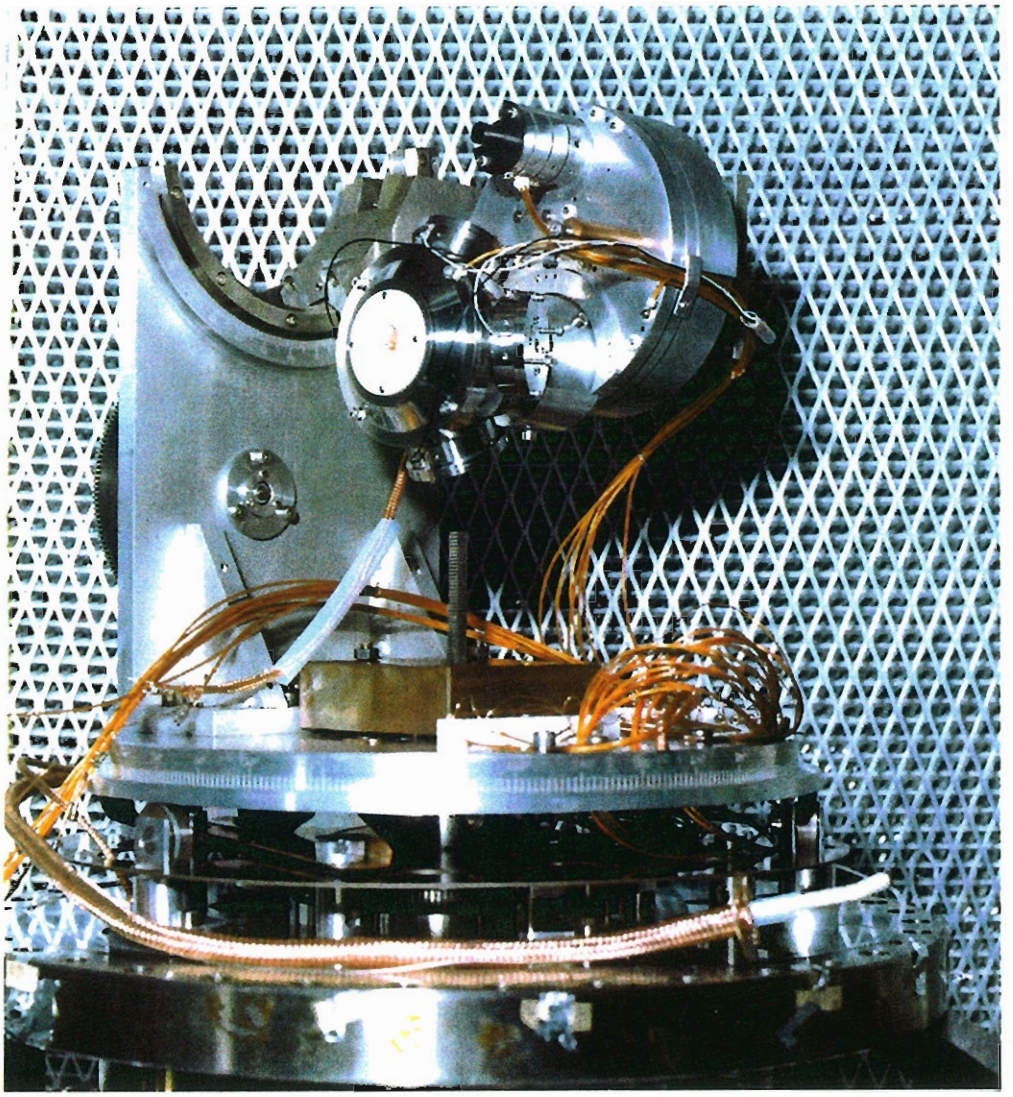

Figure 8 : Photograph of the Polarimeter/Analyser Assembly Mounted on a Two-Circle Goniometer

The data acquisition chain used with the Micro-Mott polarimeter is shown in Fig. 9. It is essentially very similar to that used on Station 1.2 except that there are only four counting channels (the Micro-Mott has no forward monitor detectors, only four backward polarisation detectors) and there is no requirement to use optical coupling (as the chamber is at earth potential).

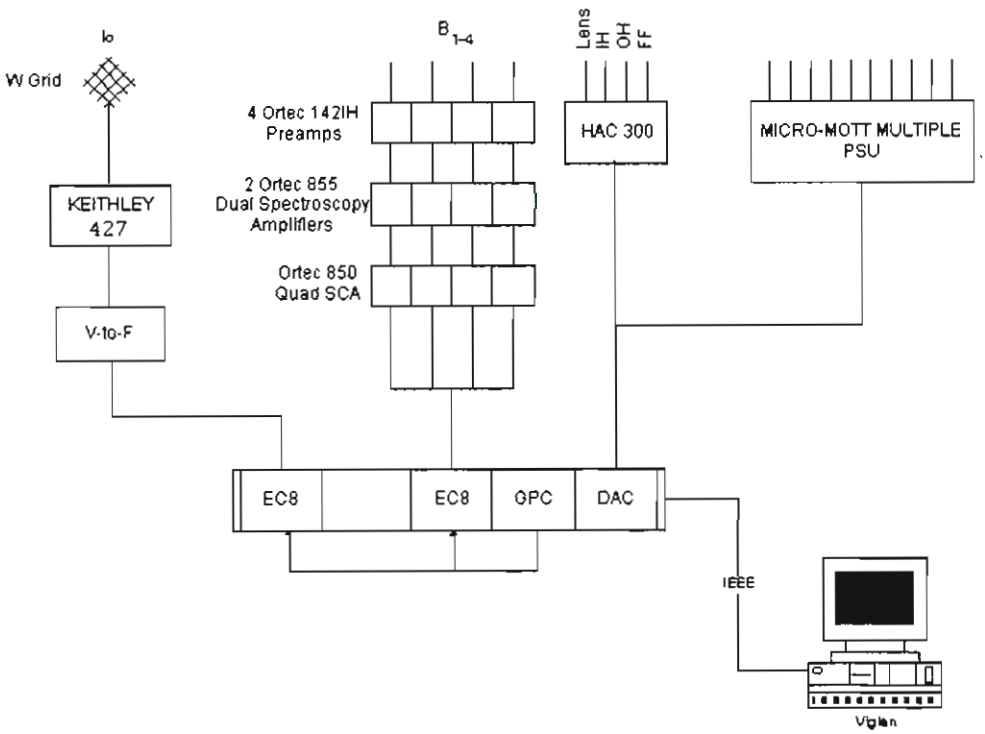

Figure 9 : Schematic Representation of the Data Acquisition Chain for the Micro-Mott Facility

4 Measurement of Electron Polarisation using the Mott Scattering Technique

4.1 General Principles of the Technique

As already discussed, the basis of the Mott scattering technique is that polarised electrons, back-scattered from a thin-gold foil, show a left-right asymmetry when measured with a pair of detectors placed in the backscattering direction at equal polar but opposite azimuthal angles to the direction of propagation of the beam. The horizontal component of P in the transverse plane (*i.e.*, in the plane orthogonal to the direction of incidence of the electrons on the foil) is determined from the asymmetry observed between the two vertically oriented detectors. Similarly, the vertical component of P in the transverse plane is determined from the asymmetry observed between the two horizontally oriented detectors (reference back to the schematic in Fig. 2 should help to clarify this). Mott scattering is insensitive to any component of polarisation along the longitudinal direction of the beam. Thus,

$$A_V = S_{eff} \cdot P_V = (T-B)/(T+B) \quad [3a]$$

$$A_H = S_{eff} \cdot P_H = (L-R)/(L+R) \quad [3b]$$

where T, B, L and R are the counts seen in the top, bottom, left and right polarisation detectors respectively.

In an ideal experiment, with identical detectors and perfect alignment of all the equipment, a single measurement of L and R, for example, would allow A_H, and therefore P_H, to be calculated directly. In practice, however, there are detector and other instrumental asymmetries which lead to L and R being different even when an unpolarised electron beam is being studied. In fact, the success of a spin-resolved photoemission measurement depends to a very large degree on the extent to which such instrumental effects can be minimised or corrected for.

4.2 Use of Magnetisation Reversal to Correct for Instrumental Asymmetry

Consider the arrival of the electron beam at the gold foil in Fig. 2, and the count rates seen in a pair of polarisation detectors placed at equal polar but opposite azimuthal angles to the beam. The system can be considered to be susceptible to misalignments of at least two kinds:

- Lateral movements of the electron beam. Such movements cause the scattering point on the foil to move closer to one detector, thereby increasing the count rate in that detector and decreasing the count rate in the other detector.
- Directional changes of the electron beam. If the electron beam arrives at the foil with a different angle of incidence, the azimuthal angle from the scattering point to the two detectors will no longer be the same, resulting in an asymmetry.

The two effects outlined above could be such as to reinforce or to cancel each other. The fact that a system exhibits zero instrumental (or *false*) asymmetry at one instance, therefore, does not guarantee that it is aligned correctly. Subsequent small changes in foil position or electron beam orientation could lead to discernible instrumental effects, thus negating the value of any data taken. In fact, relatively small changes in the electron beam trajectory can lead to significant changes in the instrumental asymmetry. This means that it is impossible to measure a system's false asymmetry once and for all. Rather, the instrumental asymmetry has to be corrected for at each individual measurement taken.

Rearranging Equation 1, it is found that the ratio of count rates seen in the left and right detectors for an electron beam of polarisation, P, is given by:

$$(L/R) = (1 + A) / (1 - A) \qquad [4]$$

Where A is derived from P using Equation 2. Modifying this to account for the relative detector efficiencies, δ, and the 'false' instrumental asymmetry introduced by misalignments, A_F, we get:

$$(L/R) = \delta \, . \, [(1 + A)/(1 - A)] \, . \, [(1 + A_F)/(1 - A_F)] \qquad [5]$$

To eliminate the A_F and δ terms in this expression, an experimental technique has been devised in which the left and right count rates are measured both for electrons with a given polarisation and also for electrons with the same characteristics but of opposite polarisation.

This procedure involves magnetising the sample fully in one sense, performing a scan, then reversing the magnetisation (and therefore the orientation of electron polarisation) and performing another identical scan. Denoting the count rates in the two detectors for the former case as $L_\uparrow$ and $R_\uparrow$, and for the latter case as $L_\downarrow$ and $R_\downarrow$, we find that:

$$(L_\uparrow/R_\uparrow) = \delta \, . \, [(1 + A)/(1 - A)] \, . \, [(1 + A_F)/(1 - A_F)] \qquad [6]$$

and

$$(L_\downarrow/R_\downarrow) = \delta \, . \, [(1 - A)/(1 + A)] \, . \, [(1 + A_F)/(1 - A_F)] \qquad [7]$$

Note the assumption here that the 'true' asymmetry, A, induced by the polarisation of the electrons, reverses sign, whilst the 'false' asymmetry, A_F, caused by instrumental effects, is unchanged. This is equivalent to saying that the trajectory of the electrons through the equipment is completely spin-independent. Combining these two equations, both δ and A_F can be eliminated. It is found that:

$$A = (X - 1) / (X + 1) \qquad [8]$$

where:

$$X = \sqrt{} \, [(L_\uparrow R_\downarrow)/(L_\downarrow R_\uparrow)] \qquad [9]$$

Knowledge of S_{eff} (determined separately) therefore leads to the polarisation, P.

Several assumptions have been made:

- That the polarisation vector of the electron beam has been precisely reversed in direction by reversing the magnetisation of the sample.
- That reversing the polarisation of the beam does not alter its trajectory through the instrument.
- That no instrumental changes have taken place between the two scans; e.g., the photons from the beamline have not varied in direction, the bending magnet current has remained constant, the relative detector efficiencies has not drifted *etc*.

One way to reduce any problems that could be caused by instrumental changes between the two scans is to switch the magnetisation of the sample at each individual point in the scan; the possibility of doing this is currently being examined.

As is evident from Fig. 2, there are four polarisation detectors, each opposing pair of which is sensitive to one of the two transverse components of the electron polarisation. When the polarisation has components in both the horizontal and vertical planes, asymmetries are therefore detected in both pairs of detectors simultaneously.

4.3 Use of Monitor and On-Axis Detectors

In addition to the backward scattering (polarisation) detectors the polarimeter on Station 1.2 also has four detectors placed in front of the gold foil, at a polar angle such that spin dependent asymmetry effects are insignificant. These detectors do of course show

instrumental asymmetries, which can be corrected for in an identical manner to that described for the polarisation detectors. When such a correction is made, these monitor detectors should show zero residual 'true' asymmetry, and this has in fact been found to be the case. The station also has a 'straight-through' detector, placed directly on the axis of the device, from which a high-count rate measure of the spin-integrated photoelectron spectrum can be obtained.

4.4 Estimation of Errors

In this section the statistical errors in the calculation of the asymmetry will be considered; *i.e.*, the uncertainties arising from the finite counting statistics involved in the measurements. Other sources of error, such as the use of an incorrect value for the Sherman Function or an invalid correction for 'false' asymmetry effects, must be assessed and estimated separately.

Consider Equation 9:

$$X = \sqrt{[(L_\uparrow R_\downarrow)/(L_\downarrow R_\uparrow)]}$$

The error in X which would arise from an error in $L_\uparrow$ (with $L_\downarrow$, $R_\downarrow$ and $R_\uparrow$ being assumed for the moment to be 'correct'), is obtained from the partial differentiation of X with respect to $L_\uparrow$. Thus:

$$\delta X/\delta L_\uparrow = 0.5 \, . \, [(L_\uparrow R_\downarrow)/(L_\downarrow R_\uparrow)]^{-1/2} \, . \, R_\downarrow / (L_\downarrow R_\uparrow)$$

$$= 0.5 \, . \, \sqrt{[R_\downarrow/(L_\uparrow L_\downarrow R_\uparrow)]}$$

therefore, the error which would arise in X, $\Delta X(L_\uparrow)$, due to an actual error in $L_\uparrow$, $\Delta L_\uparrow$, is given by:

$$\Delta X(L_\uparrow) = \Delta L_\uparrow \, . \, \sqrt{[R_\downarrow/(L_\uparrow L_\downarrow R_\uparrow)]} / 2 \qquad [10a]$$

Similarly:

$$\Delta X(R_\downarrow) = \Delta R_\downarrow \, . \, \sqrt{[L_\uparrow/(R_\downarrow L_\downarrow R_\uparrow)]} / 2 \qquad [10b]$$

$$\Delta X(L_\downarrow) = - \Delta L_\downarrow \, . \, \sqrt{[(L_\uparrow R_\downarrow)/(R_\uparrow L_\downarrow^3)]} / 2 \qquad [10c]$$

$$\Delta X(R_\uparrow) = - \Delta R_\uparrow \, . \sqrt{[(L_\uparrow R_\downarrow)/(R_\uparrow^3 L_\downarrow)]} / 2 \qquad [10d]$$

Assuming the errors arising in $L_\uparrow$, $L_\downarrow$, $R_\uparrow$ and $R_\downarrow$ are independent of each other, and assuming poissonian statistics such that the likely one standard deviation uncertainty in a measurement, N, is $\sqrt{N}$, a reasonable estimate of the likely resultant error in X can be obtained from the quadratic sum of the individual errors involved. Thus:

$$\Delta X = 0.5 \, . \, [(R_\uparrow L_\downarrow R_\downarrow + L_\uparrow L_\downarrow R_\uparrow + L_\uparrow R_\downarrow R_\uparrow + L_\uparrow R_\downarrow L_\downarrow)/(R_\uparrow^2 L_\downarrow^2)]^{1/2} \qquad [11]$$

Using similar arguments for Equation 8, it is found that the resultant error in A, ΔA, is:

$$\Delta A = 2 \, . \, \Delta X / (X + 1)^2 \qquad [12]$$

4.5 Removal of Unwanted Background from the Data

In addition to removing instrumental asymmetries by the above method, the measured asymmetries will also be affected by spurious background signals arising principally from higher order radiation in the incident photon beam, electron scattering from the Lexan support, and electrons scattered from components within the polarimeter chamber. In the data reported below account has been taken of the first two of these sources of background.

4.6 Calculation of Spin-Resolved Spectra from Polarisation Data

Having calculated the polarisation of electrons emitted by the sample at each energy in a scan, it is possible to then further calculate the spin-resolved spectra from the measured spin-integrated spectra. For Station 1.2 the spin-integrated spectrum is taken to be that measured by the 'straight-through', forward on-axis, detector; for the Micro-Mott the spin-integrated spectrum is taken to be the sum of the counts recorded at each energy by the four polarisation detectors.

Taking the spin-integrated intensity at a particular energy to be I_o, and taking the measured electron polarisation at that same energy to be P, the spin-resolved intensities (up and down) can be calculated from:

$$I_{\downarrow} = I_o \,.\, (1 - P) \qquad [13a]$$

$$I_{\uparrow} = I_o \,.\, (1 + P) \qquad [13b]$$

(Note that by definition $I_o = I_{\downarrow} + I_{\uparrow}$).

Examples of spin-integrated and spin-resolved spectra are given in section 6.2.

4.7 Determination of the Sherman Function

Clearly, having established the 'true' asymmetry from the back scattered electron counts, the degree of polarisation responsible for that asymmetry can be determined using Equation 2. To apply this equation, however, it is necessary to have an estimate of the effective Sherman Function. That is, the Sherman Function appropriate for the foil and operating conditions used during the measurements. The various methods used to establish Sherman Functions have been reviewed in detail by Gay[14] and only those relevant to the high-energy Mott polarimeter and the Micro-Mott polarimeter will be considered here.

Determination of S_{eff} for the high energy Mott polarimeter operating with an electron beam of unknown polarisation requires measurement of the scattering asymmetries as a function of scattering foil thickness and then extrapolation of the asymmetry data to zero foil thickness where a theoretical value of S_{eff}=0.39 may be assumed. At present, the range of foils available in the polarimeter is insufficient to allow an accurate extrapolation to be undertaken. However, comparison of the data described below with equivalent data obtained by Kisker and co-workers[15] [16] gave a value of S_{eff}=0.26 for the thickest foil (1000Å).

Determination of S_{eff} for the Micro-Mott polarimeter requires the measurement of the scattering asymmetries as a function of the energy window. By discriminating gradually more

and more effectively against inelastically scattered electrons it is possible to arrive at a situation approximating to single atom scattering.

So far no attempt has been made to establish the S_{eff} for the Micro-Mott polarimeter, rather the values determined in the careful work reported by Dunning *et al.*[17] have been assumed. These workers found that to the 10% precision level the effective Sherman Functions obtained for Micro-Mott polarimeters of their standard design were remarkably consistent; at 20 keV and zero energy loss window the value of S_{eff} obtained was 0.26.

Another approach to determining the Sherman Function of a system is to use a secondary standard. This is a sample which under specified conditions produces photoelectrons of known polarisation. Measuring the asymmetry from such a sample, and knowing the polarisation, allows the Sherman Function to be calculated directly from Equation 2. A number of materials have been proposed as secondary standards. For example, Hopster[18] has suggested the use of $Fe_{82}B_{12}Si_6$, $Fe_{60}Ni_{20}B_{20}$, or $Fe_{44}Ni_{37}B_{19}$ which have 20 eV secondary electron polarisations of 15-22%. And Klebanoff[19] has recommended the use of $Co_{66}Fe_4Ni_1B_{14}Si_{15}$. which has a 30 eV secondary electron polarisation of 8.5±0.010%. Although possessing a relatively low polarisation, the Co_{66} glass has been found to give very reproducible results. Further work is currently underway to develop a good secondary standard for use with the Daresbury facilities.

5 Acquisition and Analysis of Spin-Resolved Data from Station 1.2 and the Micro-Mott

A common data acquisition and control program is used for the collection of data from Station 1.2 and the Micro-Mott facility. In addition, utilities are available for the further analysis and display of this data, both on- and off-line (*i.e.*, at data collection time on the station control computer, or at a later stage on a different machine). More detailed information is reported elsewhere[11].

The procedure adopted for acquiring spin-resolved data has been described in Section 4.2. A scan (or a set of multiple scans) is performed with a given sample magnetisation, the magnetisation is then reversed, and an identical set of scans is then obtained. During scanning a graphical display is available to the user, and a choice of screens (selectable using the computer keyboard function keys) show the counts obtained from the various detectors, or the calculated asymmetry information, plotted against energy. (Note that it is not possible to calculate and display 'true' asymmetries, corrected for instrumental effects, until the whole data collection run, at both magnetisations, is completed.) The screens available during scanning are as outlined below:

screen 1: Counts from the straight-through (forward, on-axis) detector vs. energy.
screen 2: Counts from each of the four backward (polarisation)detectors vs. energy.
screen 3: Counts from each of the four forward (monitor) detectors vs. energy.
screen 4: Counts from the I_o reference channel vs. energy.
screen 5: Calculated (uncorrected) asymmetries from the two pairs of backward (polarisation) detectors. Two curves are plotted, showing (L-R)/(L+R) and (T-B)/(T+B), as outlined in Section 4.1. These displays show the combined

instrumental and spin asymmetries of the system. They do not necessarily reflect any resultant 'true' asymmetries that may subsequently be calculated.

screen 6: Calculated (uncorrected) asymmetries from the two pairs of forward (monitor) detectors. Two curves are plotted, showing (L-R)/(L+R) and (T-B)/(T+B), as outlined in Section 4.1. These displays show essentially the instrumental asymmetry in the system.

Note that count *rates* are plotted; *i.e.,* counts collected per unit time. This allows scans performed with differing integration times to be more easily compared with each other.

Having taken and stored these datasets, options are then available from the menu of the main data acquisition program to compare them, eliminate instrumental asymmetries, and thus calculate 'true' asymmetries. These are:

1) *Average Datasets*: This prompts for the run numbers of the individual scans taken at a given magnetisation, reads their contents, sums the individual counts recorded from each detector at each energy, and writes out a single new datafile containing the counts averaged over the number of files summed. Note that in order to preserve information about counting statistics the number of scans over which the average was made is recorded in the header of the new file created. A large number of individual scan files therefore reduce to a more easily manageable two (one for each magnetisation). These files can then be specified as the input files to the next option:

2) *Calculate Polarisation*: This option prompts the user for either the names of a pair of datafiles created by the 'average datasets' option, or for the run number ranges of the sets of files acquired at each of the two magnetisations. In the latter case the option will then perform a summation identical to that carried out by the average datasets option. It is not therefore strictly necessary to run the average datasets option before running the calculate polarisation option; the only benefit of doing so is that the whole of a data collection run can be summarised in just a pair of files. Having summed all the data available from a sample at each magnetisation, the program then calculates the 'true' asymmetry at each energy in the scan using the equations specified in Section 4.2. This is done for four pairs of detectors: the polarisation detectors in the horizontal plane, the polarisation detectors in the vertical plane, the monitor detectors in the horizontal plane, and the monitor detectors in the vertical plane. In principle, if instrumental effects have been successfully removed, the 'true' asymmetries calculated from the two pairs of monitor detectors should be zero. (Note that the program plots error bars calculated using Equations 10, 11 and 12 at each point; and any residual 'true' asymmetries can therefore be assessed for statistical significance.) The user is prompted for a value to adopt for the Sherman Function, and the asymmetries are converted to polarisation using Equation 2 before being plotted to the screen. A further option also allows the spin-resolved photoemission spectra to be calculated using Equations 13a and 13b and displayed to the screen.

In addition to the options provided on the station, the above utilities are also available as an off-line program known as *spscalc*. Currently this resides on the Surface Science village computer, SSCPU1, and can be accessed by users logged on through the site X-server, XSERV1, using the command *sscs spscalc*. The program reads in and processes datafiles collected from both Station 1.2 (SPS1) and the Micro-Mott (SPS2), and produces text-based output files suitable for subsequent analysis by packages such as MOTPLOT or PLOTEK. It

is intended, in the near future, to replace this 'stand-alone' program with an easier to use option under the Surface Science Shell. This will not only have a graphical user interface (GUI), but will provide more sophisticated in-built plotting and hard copy facilities.

6 Results

6.1 Example I: Nickel(110)

Some preliminary normal-photoemission asymmetry results of the valence band of nickel (110), obtained using Station 1.2, are shown in Fig. 10. A photon energy of 16.85eV was used with the beam oriented at 45° to the surface normal. Typical count rates obtained for the peak of the valence band with a low resolving power were $5x10^4$cps in the straight-through detector and $8x10^2$cps in each of the polarisation detectors. An accumulation time of approximately two hours was required for moderate counting statistics. Great care was taken with the magnetisation of the nickel, this being achieved by passing a current pulse of approximately 120A and 150μs duration through a copper coil wrapped four and a half times around one of the legs of the picture frame. The magnitude of the current required to saturate the sample was estimated from off-line magneto optical Kerr effect (MOKE) measurements.

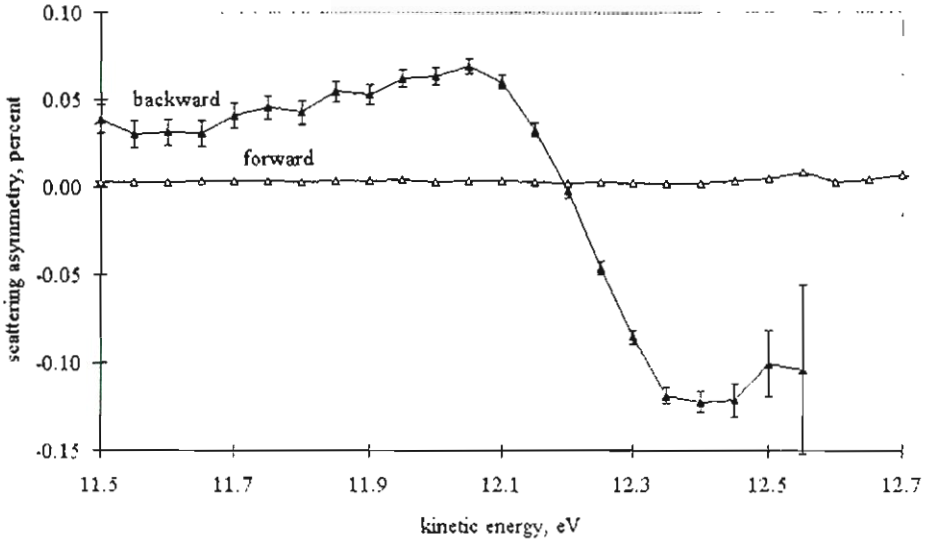

Figure 10 : (A) The Photoemission Spin Asymmetry of the d-band Region of Ni(110).

The spin-dependent asymmetries obtained from the two pairs of backward (polarisation) and forward (monitor) detectors are shown in Fig. 10. The backward scattering data clearly show a statistically significant spin-dependent scattering asymmetry that is absent in the forward direction. This absence of significant asymmetry in the forward direction, in agreement with theoretical expectations, generates a degree of confidence that the procedure adopted for removing the instrumental effects, as outlined above, is valid.

6.2 Example II: $Fe_{80}B_{20}$ Amorphous Alloy

Some photoemission results on the glassy alloy $Fe_{80}B_{20}$ obtained using the MicroMott Facility on Station 6.1 are shown in Fig. 11. The data were obtained at room temperature on a

sample that had been sputter cleaned but not annealed. A photon energy of 110eV was used with the photon beam oriented at 45° to the surface normal (the photoemission direction). The peak count rate obtained for the valence band was 45cps and an accumulation time of approximately 24 hours was required to obtain the data. The polarisation obtained from the two pairs of polarisation detectors (assuming a Sherman Function of 0.15) are shown in Fig. 11(B). The data clearly show significant horizontal polarisation and negligible vertical polarisation components. This is expected because the alloy sample was magnetised in the horizontal plane. The spin resolved d-band spectra are shown in Fig. 11(C). A more complete account of these results and their interpretation can be found elsewhere[20].

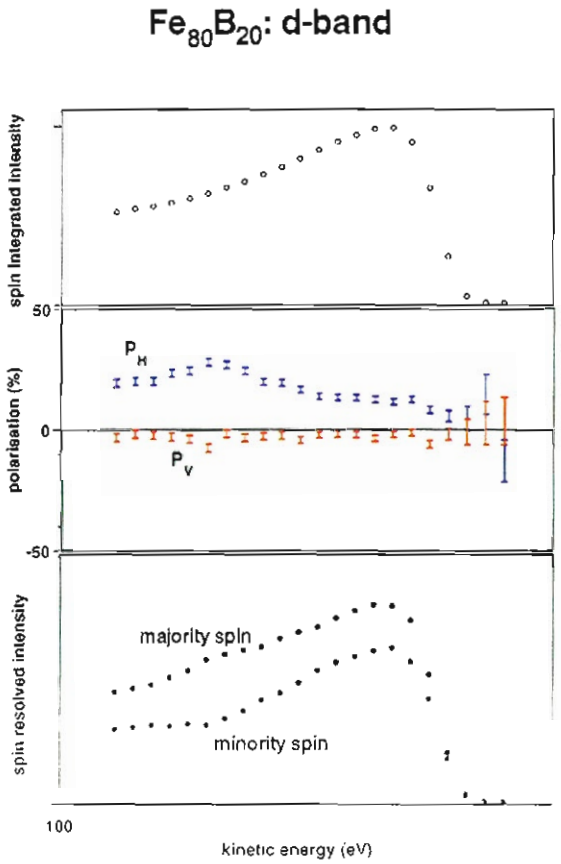

Figure 11 : (A) The Spin Integrated Photoemission Spectra of the d-band region of $Fe_{80}B_{20}$; (B) The Polarisation over the Same Region; (C) The Spin-Resolved Spectra

7 Acknowledgements

We would like to thank DL for the provision of funds to construct and support the Micro-Mott Facility. In addition, we are happy to acknowledge the expert assistance provided in support of this project by the staff of DL and fruitful discussions with Dr Mike Hardiman (Sussex University).